Electromagnetic Performance Comparison of Pole-Slot Combination in Outer Rotor Permanent Magnet Synchronous Machine for Drone Application

Hyunwoo Kim
Elmore Family School of Electrical and Computer Engineering
Purdue University
West Lafayette, IN, USA
kim4852@purdue.edu

Woongkul Lee
Elmore Family School of Electrical and Computer Engineering
Purdue University
West Lafayette, IN, USA
wklee@purdue.edu

***Abstract*—Outer rotor permanent magnet synchronous motors (ORPMSMs) have received attention for drone application due to their high-power density and integration of the propeller blade onto the rotor. In this paper, electromagnetic performance of ORPMSMs is compared for various pole-slot combinations with a fractional slot concentrated winding. Based on the basic model with 42-poles and 36-slots, two case studies are conducted to obtain the superior electromagnetic performance of pole-slot combination using finite element analysis (FEA). In the first case study, pole-slot combinations with identical pole-to-slot ratios are analyzed, and the results show that an optimal pole number exists even when the ratio remains constant. In second case study, the electromagnetic performance is evaluated for different pole numbers while maintaining the same slot number. The results provide guidance for selecting the optimal pole-slot combination considering the power density and efficiency.**

***Index Terms*—Efficiency, electromagnetic performance, outer rotor permanent magnet synchronous motor (ORPMSM), pole-slot combination, power density.**

I. INTRODUCTION

Surface permanent magnet synchronous motors (SPMSMs) have gained significant attention in the drone application. In particular, the outer rotor PMSMs (ORPMSMs) employing surface magnets offer the benefit of high pole number, which can achieve the high power density [1]. Furthermore, because SPMSMs have a relatively large effective magnetic airgap, the eddy current loss in the rotor yoke is lower. For this reason, the rotor yoke of ORPMSMs with surface magnets is widely manufactured as the solid core material like SUS304 or SS400, as illustrated in Fig. 1 [2]. This structure enables integration of the propeller blade onto the rotor without an additional housing, resulting in a simplified manufacturing process. Owing to these benefits, ORPMSMs have been employed in the drone application.

Although ORPMSMs provide superior electromagnetic performance compared with other motor topologies in the drone application, their power density and electromagnetic loss characteristics depend on the pole-slot combination. Specifically, since ORPMSMs have a fractional slot concentrated winding and the rotor yoke is solid material this structure can cause the higher eddy current loss in the rotor yoke. Therefore, the selection of pole-slot combination is significant design step before starting the geometry design of electrical machine. Since ORPMSMs with SPMSM have the eddy current loss in the rotor yoke depending on the stator magnetomotive force (MMF), electromagnetic performance should be investigated for winding configuration of pole-slot combination [3].

Several research have been studied on the electromagnetic characteristics of various pole-slot combinations [4]-[7]. In [4], electromagnetic performance for pole-slot combination in interior PMSM is investigated for electric power steering. In [5]-[6], the vibration characteristics for pole-slot combination are focused. Although the pole-slot combination of ORPMSM is investigated in [7]-[8], electromagnetic performance is focused on the amount of permanent magnet material and low speed and high torque density application. Despite these prior works, no study has specifically addressed the power density and efficiency, which are significant performance in drone applications, for pole-slot combinations.

In this paper, electromagnetic performance for pole-slot

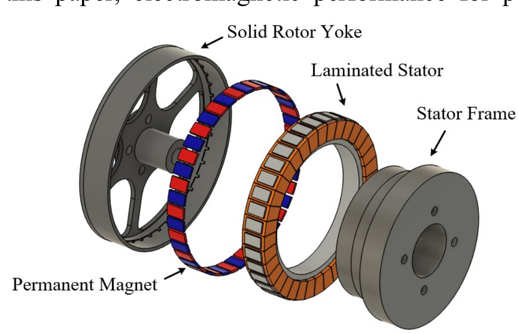

Figure 1. Configuration of ORPMSM for drone application.

979-8-3315-8138-1

combination of ORPMSMs is investigated for the drone application. Because ORPMSMs employ a solid rotor yoke, the winding configuration for pole-slot combinations significantly affects the loss characteristics. Moreover, the efficiency and power density are key performance metrics in the drone applications, two case studies for pole-slot combination are conducted in term of efficiency and power density: Case I: pole-slot combination with an identical pole-slot ratio, and Case II: variations in pole number for the fixed slot number. Based on the basic model of 42 poles and 36 slots, which is used in the drone application, two case studies are conducted and electromagnetic performance for case studies is compared based on finite element analysis (FEA).

II. Selection of Pole-Slot Combinations

The pole-slot combination significantly influences electromagnetic characteristics, including the winding factor, the back electromagnetic force (BEMF), motor period, and cogging torque. The winding configuration associated with a given pole-slot combination is determined by the start of slot theory [9]. Based on this theory, the characteristics of pole-slot combination can be predicted in advance during motor design process.

A. Winding Feasibility and Winding Factor

Based on the star of Slot theory, the winding feasibility is determined given pole-slot combination as follows:

$$\frac{Q}{mt} = \text{int}. \tag{1}$$

where Q is the slot number, m is the number of phases, t is the motor period. The motor period can be expressed as follows:

$$t = GCD(Q,\ p) \tag{2}$$

where GCD is the greater common divider (GCD), p is the number of pole pair.

The BEMF of electrical machines can be expressed as follows:

$$E = \omega_e k_w N_w \phi_g \tag{3}$$

where E is the BEMF, ω_e is the electrical angular speed, k_w is the winding factor, N_w is the series turns per phase, and ϕ_g is the airgap magnetic flux. From (3), the winding factor determines the BEMF, and a higher winding factor results in a higher torque because the BEMF is proportional to the torque. The winding factor is defined by the product of distribution factor and pitch factor as follows:

$$k_w = k_d k_p \tag{4}$$

where k_d is the distribution factor and k_p is pitch factor.

The distribution factor can be expressed as follows [10]:

$$k_d = \begin{cases} \dfrac{2\sin\dfrac{\pi}{2m}}{q_{ph}\sin\dfrac{\alpha_{ph}}{2}} & \text{when } \dfrac{Q}{mt} = even \\[2ex] \dfrac{\sin\dfrac{\pi}{2m}}{q_{ph}\sin\dfrac{\alpha_{ph}}{4}} & \text{when } \dfrac{Q}{mt} = odd \end{cases} \tag{5}$$

TABLE I. Winding Factor for Pole-Slot Combinations

Winding Factor		Slot Number									
		24	27	30	33	36	39	42	45	48	51
Pole Number	28	0.933	0.954	0.951	0.928	0.888	0.863	0.866	0.792	0.760	0.725
	30		0.945			0.933			0.866		
	32	0.866	0.915	0.951	0.954	0.945	0.917	0.890	0.858	0.866	0.796
	34	0.760	0.877	0.931	0.954	0.953	0.936	0.911	0.886	0.857	0.866
	36		0.866								
	38	0.583	0.766	0.869	0.928	0.953	0.954	0.937	0.927	0.905	0.880
	40	0.500	0.695	0.866	0.903	0.945	0.954	0.953	0.945	0.933	0.901
	42		0.617			0.933			0.951		
	44	0.250	0.525	0.711	0.866	0.888	0.936	0.953	0.955	0.949	0.933

TABLE II. LCM of Pole and SLot Number for Pole-Slot Combinations

LCM		Slot Number									
		24	27	30	33	36	39	42	45	48	51
Pole Number	28	168	756	420	924	252	1092	84	1260	336	1428
	30		270			180			90		
	32	96	864	480	1056	288	1248	672	1440	96	1632
	34	408	918	510	1122	612	1326	714	1530	816	102
	36		108								
	38	456	1026	570	1254	684	1482	798	1710	912	1938
	40	120	1080	120	1320	360	1560	840	360	240	2040
	42		378			252			630		
	44	264	1188	660	132	396	1716	924	1980	528	2244

where q_{ph} is the number of spokes per phase, and α_s is the angle between two consecutive phasors of the star of slots.

The pitch factor can be expressed as follows:

$$k_p = \sin\frac{\pi p y_q}{Q},\ y_q = \max\left(\frac{Q}{2p},\ 1\right). \tag{6}$$

where y_q is the slot pitch. Since the fractional slot concentrated winding machine is widely employed in the drone application, the slot pitch is selected as one.

Based on (5) and (6), the winding factor for pole-slot combinations can be calculated for the fractional slot concentrated winding machine, as illustrated in TABLE I. In TABLE I, a blank entry indicates that the winding configuration is not feasible for a three-phase winding. Since the pole-slot combination with higher winding factor produce the higher BEMF according to (3), these combinations are generally preferred. However, electromagnetic performance characteristics such as cogging torque and noise/vibration are influenced by the least common multiple (LCM) and great common multiple (GCD) of pole and slot number. Therefore, additional factors must be considered when selecting the pole-slot combination. In particular a higher pole number can increase the switching frequency in the motor drive and core loss. Accordingly, electromagnetic performance of the selected pole-slot combination candidates should be evaluated using FEA. Based on these comparative results, the optimal pole-slot combination can be identified.

B. LCM and GCD of Pole-Slot Combinations

In PMSMs, the cogging torque is generated by the variation of magnetic permeance and is influenced by pole-slot combination, as the cogging torque period is determined by LCM of pole and slot numbers, as illustrated in TABLE II. Therefore, selecting an appropriate pole-slot combination is an essential part of the initial design process when targeting low cogging torque. In general, pole-slot combination with larger LCM tend to exhibit lower cogging torque [15]. However, although a higher LCM number typically reduces cogging torque, the actual cogging torque is also affected by various design parameters, including the slot opening, skew, and magnet shape. Therefore, the pole–slot combination provides an initial guideline for achieving low cogging torque, while further reduction can be obtained through geometric design.

TABLE III. GCD OF POLE-PAIR AND SLOT NUMBER FOR POLE-SLOT COMBINATIONS

GCD		Slot Number									
		24	27	30	33	36	39	42	45	48	51
Pole Number	28	2	1	2	1	2	1	14	1	2	1
	30		3			3			15		
	32	8	1	2	1	4	1	2	1	16	1
	34	1	1	1	1	1	1	1	1	1	17
	36		9								
	38	1	1	1	1	1	1	1	1	1	1
	40	4	1	10	1	4	1	2	5	4	1
	42		3			3			3		
	44	2	1	2	11	2	1	2	1	2	1

TABLE IV. *Q*/(*MT*) FOR POLE-SLOT COMBINATIONS

Q/(mt)		Slot Number									
		24	27	30	33	36	39	42	45	48	51
Pole Number	28	4	9	5	11	6	13	1	15	8	17
	30		3			4			1		
	32	1	9	5	11	3	13	7	15	1	17
	34	8	9	10	11	12	13	14	15	16	1
	36		1								
	38	8	9	10	11	12	13	14	15	16	17
	40	2	9	1	11	3	13	7	3	4	17
	42		3			4			5		
	44	4	9	5	1	6	13	7	15	8	17

TABLE V. SPECIFICATION FOR DRONE APPLICATION

Contents	Value	Contents	Value
Power [W]	600	Stack length [mm]	8.5
Speed [rpm]	3000	Airgap length [mm]	0.5
Torque [Nm]	1.91	Slot opening [mm]	2
Phase current [A_{max}]	20	Magnet thickness [mm]	1.1
Total series turns	120	Stator core material	50PN470
Wire diameter [mm]	0.8	Rotor yoke material	SS400

Noise/vibration of electrical machine is caused by the radial magnetic forces in the airgap as expressed follows:

$$f(\theta, t) = \frac{1}{2\mu_0}\left[B_n^2(\theta, t) - B_t^2(\theta, t)\right] \quad (7)$$

where f is the radial magnetic force density, and B_n and B_t are normal and tangential component of magnetic flux density, respectively. If the electrical machine exhibits unbalanced magnetic pull due to its winding configuration in specific pole-slot combination, a unidirectional radial force is generated, resulting in increased noise/vibration. The electrical machine with the symmetric winding configurations typically achieves lower noise/vibration. Because GCD of pole-pair and slot number demonstrates the motor period, it can be used as the index of the symmetry. For this reason, the pole-slot combinations with even GCD are commonly selected, as shown in TABLE III. Even when GCD is odd, the symmetries in winding configurations can be achieved through the symmetric winding distribution per phase, in which one half of the winding layer is arranged as the reverse of the other half. Since the number of winding distributions per phase can be given by $Q/(mt)$, the half-symmetric winding distributions can be implemented when $Q/(mt)$ is an even number, as shown in TABLE IV.

III. CASE STUDIES OF POLE-SLOT COMBINATION

A. Constraints and Specification

To compare electromagnetic performance for pole-slot combination, the machine specification for drone application is considered as shown in TABLE V. In this paper, 42 pole and 36 slot configuration is selected as a basic model, and two case studies of pole-slot combination are conducted.

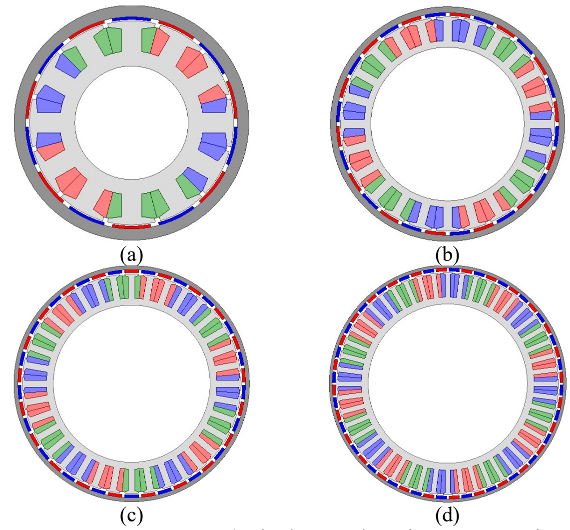

(Red : Phase A, Blue : Phase B, Green : Phase C)

Figure 2. Pole-slot combination models for Case I. (a) 14P12S. (b) 28P24S. (c) 42P36S. (d) 56P48S.

TABLE VI. DIMENSION OF POLE-SLOT COMBINATION MODELS FOR CASE I

Contents	14P 12S	28P 24S	42P 36S	56P 48S	Unit
Airgap diameter	81.15				mm
Rotor outer diameter	93.1	88.6	87.1	86.35	mm
Rotor inner diameter	81.9				mm
Stator outer diameter	80.9				mm
Stator inner diameter	45	58	58	58	mm
Rotor yoke thickness	4.5	2.25	1.5	1.125	mm
Stator teeth thickness	4.5	3.4	2.5	1.875	mm
Stator yoke thickness	5	2.5	2.5	2.5	mm
Winding factor	0.933				-
GCD(Q, p)	3				-
$Q/(mt)$	4				-
LCM(Q, p)	84	168	252	336	-

In first case study (Case I), pole-slot combinations with the same pole-to-slot ratio are selected to compare the electromagnetic performance. Since the basic model is 42-pole/36-slot configuration, the candidate combinations are chosen to maintain the same pole-to-slot ratio, as illustrated in Fig. 2. As the magnetic flux per pole increases when the pole number decreases, the stator and rotor yoke thicknesses are designed to avoid magnetic saturation while maintaining the same airgap diameter. The geometric dimensions used in Case I are summarized in TABLE VI.

In second case study (Case II), electromagnetic performance is compared using the same slot number but varying pole numbers. With the basic model employing 36 slots, the slot number is fixed at 36 for all candidate configurations. The pole number are selected based on winding feasibility and winding factor considerations, as illustrated in Fig. 3. The rotor yoke thickness is determined to prevent magnetic saturation, and the detailed geometric dimensions are listed in TABLE VII. The electromagnetic performance of the selected pole-slot combinations is evaluated under both no-load and load conditions using FEA of which software is ANSYS Maxwell 2024R1.

979-8-3315-8138-1

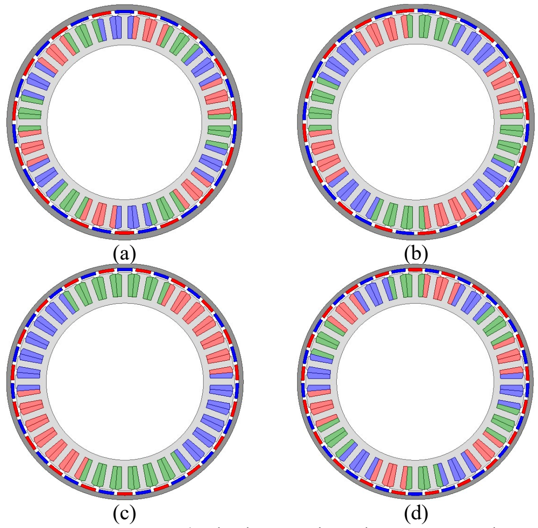

(Red : Phase A, Blue : Phase B, Green : Phase C)
Figure 3. Pole-slot combination models for Case II: (a) 30P36S. (b) 32P36S. (c) 38P36S. (d) 42P36S.

TABLE VII. DIMENSION OF POLE-SLOT COMBINATION MODELS FOR CASE II.

Contents	30P 36S	32P 36S	38P 36S	42P 48S	Unit
Airgap diameter	81.15				mm
Rotor outer diameter	88.3	88.04	87.42	87.1	mm
Rotor inner diameter	81.9				mm
Stator outer diameter	80.9				mm
Stator inner diameter	58	58	58	58	mm
Rotor yoke thickness	2.1	1.97	1.66	2.5	mm
Winding factor	0.933	0.945	0.953	0.933	-
GCD(Q, p)	3	4	1	3	-
$Q/(mt)$	4	3	12	4	-
LCM(Q, p)	180	288	684	252	-
Stator teeth thickness	2.5				mm
Stator yoke thickness	2.5				mm

B. *Case I : Same Ratio of Pole and Slot Number*

Although the pole-to-slot ratio is identical, electromagnetic performance varies with the pole number due to the magnetic flux per pole and leakage flux. As the pole number increases, the magnetic flux per pole decreases, leading to a reduction in magnetic flux density, as illustrated in Fig. 4. This indicates that the required core usage can be reduced, thereby contributing to higher power density.

Fig. 5 presents the no-load characteristics of pole-slot combinations in Case I. As shown in Fig. 5(a), the induced voltage waveform becomes more sinusoidal as the pole number increases, primarily due to the increased leakage flux. Although a lager LCM yields lower cogging torque, the cogging torque of 42P36S is higher than that of 28P24S, as illustrated in Fig. 5(b). This confirms that the cogging torque is influenced not only by the pole-slot combination but also by the geometric features of the rotor and stator.

The load characteristics, including electromagnetic loss, output power, power density, and efficiency, are compared, as illustrated in Fig. 6. As shown in Fig. 6(a), the core loss for the pole number increases because it is proportional to both

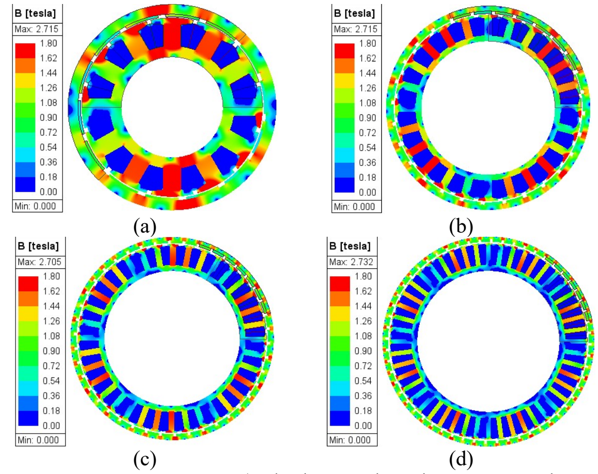

(Red : Phase A, Blue : Phase B, Green : Phase C)
Figure 4. Mangetic flux density distribution under load condition for Case I. (a) 14P12S. (b) 28P24S. (c) 42P36S. (d) 56P48S.

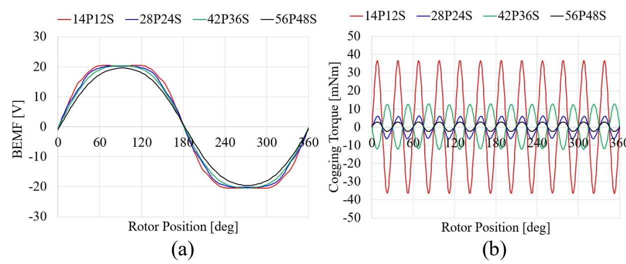

Figure 5. Noload characteristics for Case I. (a) BEMF. (b) Cogging torque.

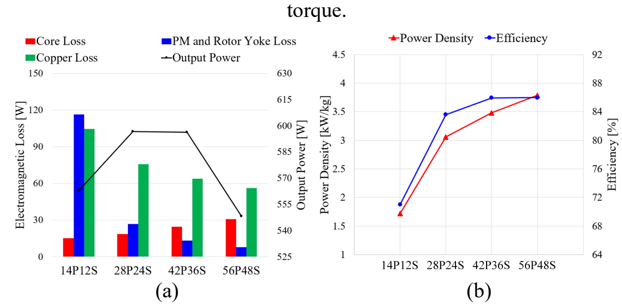

Figure 6. Load characteristics for Case I. (a) Loss and output power. (b) Power density and efficiency.

magnetic flux density and electrical frequency. Although the stack length, wire diameter, and total series turn are same across models, the end-turn resistance decreases as the slot number increases, resulting in lower copper loss, as shown in Fig. 6(a). The PM and rotor yoke loss depends on the stator MMF distribution, and spatial harmonic by slot. As shown in Fig. 6(a), the machines with fewer poles exhibit higher spatial harmonic component, leading to increased PM and rotor yoke loss. Consequently, although power density improves as the pole number increases, the efficiency of 42P36S is higher than that of other pole-slot combinations, as illustrated in Fig. 6(b).

C. *Case II : Pole Number Under Same Slot Number*

This case study is focused on evaluating the electromagnetic performance for different pole numbers while maintaining the same slot number and geometric dimensions. Similar to Case I, the magnetic flux density decreases as the pole number increases, as illustrated in Fig. 7. Because the stator geometry is fixed, the magnetic flux density in stator teeth decreases with increasing pole number.

Fig. 8 shows the no-load characteristics of pole-slot combination examined in Case II. As illustrated in Fig. 8(a), the BEMF waveforms of 30P36S and 32P36S are more sinusoidal compared to 38P36S and 42P36S. As shown in Fig. 8(b), 38P36S exhibits the higher LCM, as shown in TABLE VII, and therefore shows the lowest cogging torque. Although 30P36S model has a lower LCM compared to 42P36S, its cogging torque is higher, demonstrating that geometric parameters influence cogging torque.

The load characteristics for Case II is compared in Fig. 9. The core loss increases with the pole number increases. However, PM and rotor yoke loss increase for the high pole number, as shown in Fig. 9(a), which contrasts with the trend observed in Case I. This indicates that the winding configuration contributes to the PM and rotor yoke loss. Since the higher pole number allows for reduced core mass, power density improves as the pole number increases. Considering both electromagnetic losses and power density, the optimal pole-slot combination is selected as 38P36S.

IV. Conclusion

In this paper, the pole-slot combinations of ORPMSMs are investigated for drone applications. Because ORPMSMs employ a solid rotor yoke, eddy-current loss is generated in the rotor, and this loss is influenced by the winding configuration. Two case studies are conducted based on the basic model with 42-pole and 36-slot commonly used in drone applications. In Case I, where the pole-slot ratio is kept constant, the 42-pole and 36-slot exhibits higher power density and efficiency compared with the other models. In contract, in Case II, where the stator geometry is fixed and the pole number is varied, the 38-pole and 36-slot provides superior power density and efficiency. For drone application, higher pole numbers are generally preferred due to their high power density. However, increasing the pole number raises the required inverter switching frequency, which in turn increases switching losses and reduce the overall efficiency of the motor and drive system. Therefore, future work will investigate pole-slot combination considering both motor performance and drive system.

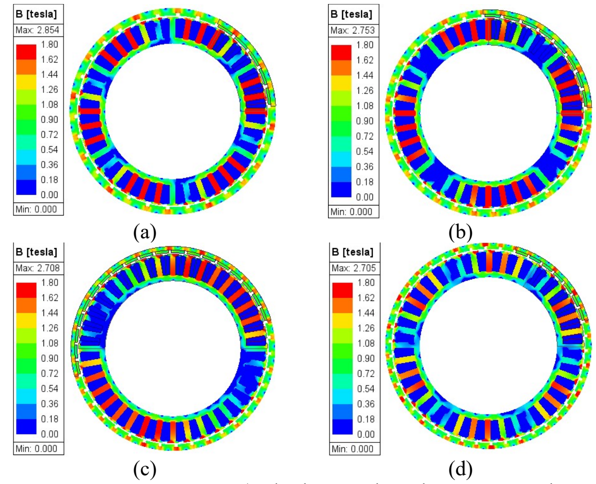

(Red : Phase A, Blue : Phase B, Green : Phase C)

Figure 7. Mangetic flux density distribution under load condition for Case II. (a) 30P36S. (b) 32P36S. (c) 38P36S. (d) 42P36S.

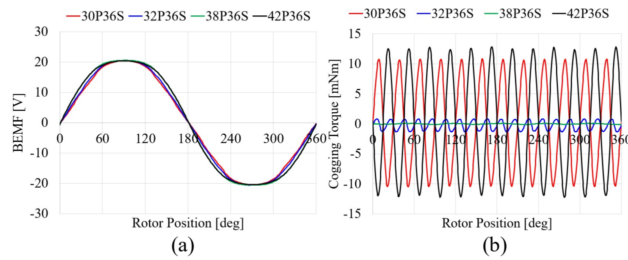

Figure 8. Noload characteristics for Case II. (a) BEMF. (b) Cogging torque.

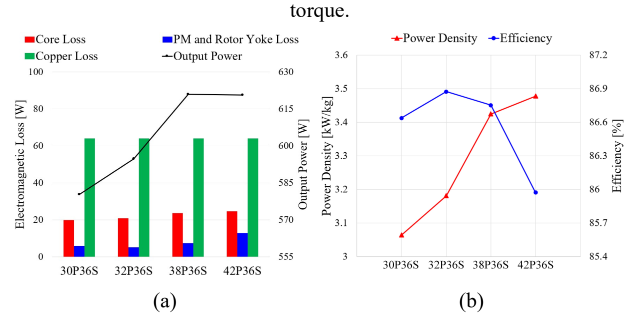

Figure 9. Load characteristics for Case II. (a) Loss and output power. (b) Power density and efficiency.

References

[1] Q. He, H. Wang and Q. Li, "Design Optimization and Performance Analysis of High Torque Density and Efficiency Motors for eVTOL Applications," *IEEE Access*, vol. 13, pp. 78403-78415, 2025.

[2] I. Petrov, M. Niemelä, P. Ponomarev and J. Pyrhönen, "Rotor Surface Ferrite Permanent Magnets in Electrical Machines: Advantages and Limitations," *IEEE Trans. Ind. Electron.*, vol. 64, no. 7, pp. 5314-5322, July 2017.

[3] E. Fornasiero, N. Bianchi and S. Bolognani, "Slot Harmonic Impact on Rotor Losses in Fractional-Slot Permanent-Magnet Machines," *IEEE Trans. Ind. Electron.*, vol. 59, no. 6, pp. 2557-2564, June 2012.

[4] E. Carraro, N. Bianchi, S. Zhang and M. Koch, "Design and Performance Comparison of Fractional Slot Concentrated Winding Spoke Type Synchronous Motors With Different Slot-Pole Combinations," *IEEE Trans. Ind. Appl.*, vol. 54, no. 3, pp. 2276-2284, May-June 2018.

[5] W. Zhao, S. Zhu, J. Ji, G. Liu and Y. Mao, "Analysis and Reduction of Electromagnetic Vibration in Fractional-Slot Concentrated-Windings PM Machines," *IEEE Trans. Ind. Electron.*, vol. 69, no. 4, pp. 3357-3367, April 2022.

[6] S. Zhu, W. Zhao, J. Ji, G. Liu and C. H. T. Lee, "Design to Reduce Modulated Vibration in Fractional-Slot Concentrated-Windings PM Machines Considering Slot–Pole Combination," in *IEEE Trans. Transport. Electrific.*, vol. 9, no. 1, pp. 575-585, March 2023.

[7] Y. Song, G. Liu, S. Yu, H. Wang and F. Zhang, "Investigation of a Low-Speed High-Torque-Density Direct-Drive External-Rotor PMSM for Belt Conveyor Application," *IEEE Access*, vol. 11, pp. 110479-110489, 2023.

[8] P. Sergeant and A. P. M. Van den Bossche, "Influence of the Amount of Permanent-Magnet Material in Fractional-Slot Permanent-Magnet Synchronous Machines," *IEEE Trans. Ind. Electron.*, vol. 61, no. 9, pp. 4979-4989, Sept. 2014.

[9] N. Bianchi, M. Dai Pre, L. Alberti, and E. Fornasiero, ´ Theory and Design of Fractional-Slot PM Machines, Sponsored by the IEEEIAS Electrical Machines Commitee, Ed. Padova: CLEUP (ISBN 978-88-6129-122-5), 2007.

[10] Z. Q. Zhu and D. Howe, "Influence of design parameters on cogging torque in permanent magnet machines," *IEEE Trans. Energy Convers.*, vol. 15, no. 4, pp. 407-412, Dec. 2000.

979-8-3315-8138-1